International Journal of Thermophysics, Vol. 24, No. 1, January 2003 (© 2003)

Non-Contact Measurements of the Thermophysical Properties of Hafnium-3 mass% Zirconium at High Temperature

P.-F. Paradis,[1,2] T. Ishikawa,[1] and S. Yoda[1]

Received December 11, 2001

Several thermophysical properties of hafnium-3 mass % zirconium, namely the density, the thermal expansion coefficient, the constant pressure heat capacity, the hemispherical total emissivity, the surface tension and the viscosity are reported. These properties were measured over wide temperature ranges, including overheated and undercooled states, using an electrostatic levitation furnace developed by the National Space Development Agency of Japan. Over the 2220 to 2875 K temperature span, the density of the liquid can be expressed as $\rho_L(T) = 1.20 \times 10^4 - 0.44(T - T_m)$ ($\mathrm{kg \cdot m^{-3}}$) with $T_m = 2504$ K, yielding a volume expansion coefficient $\alpha_L(T) = 3.7 \times 10^{-5}$ ($\mathrm{K^{-1}}$). Similarly, over the 1950 to 2500 K span, the density of the high temperature and undercooled solid β-phase can be fitted as $\rho_S(T) = 1.22 \times 10^4 - 0.41(T - T_m)$, giving a volume expansion coefficient $\alpha_S(T) = 3.4 \times 10^{-5}$. The constant pressure heat capacity of the liquid phase can be estimated as $C_{PL}(T) = 33.47 + 7.92 \times 10^{-4}(T - T_m)$ ($\mathrm{J \cdot mol^{-1} \cdot K^{-1}}$) if the hemispherical total emissivity of the liquid phase remains constant at 0.25 over the 2250 K to 2650 K temperature interval. Over the 1850 to 2500 K temperature span, the hemispherical total emissivity of the solid β-phase can be represented as $\varepsilon_{TS}(T) = 0.32 + 4.79 \times 10^{-5}(T - T_m)$. The latent heat of fusion has also been measured as 15.1 $\mathrm{kJ \cdot mol^{-1}}$. In addition, the surface tension can be expressed as $\sigma(T) = 1.614 \times 10^3 - 0.100(T - T_m)$ ($\mathrm{mN \cdot m^{-1}}$) and the viscosity as $h(T) = 0.495 \exp[48.65 \times 10^3/(RT)]$ (mPa·s) over the 2220 to 2675 K temperature range.

KEY WORDS: density; hafnium; heat capacity; hemispherical total emissivity; latent heat of fusion; liquid metal; non-contact processing; surface tension; viscosity.

[1] National Space Development Agency of Japan, Tsukuba Space Center, 2-1-1 Sengen, Tsukuba City, Ibaraki 305-8505, Japan.

[2] To whom correspondence should be addressed. E-mail: paradis.paulfrancois@nasda.go.jp

0195-928X/03/0100-0239/0 © 2003 Plenum Publishing Corporation

1. INTRODUCTION

Due to its refractory nature, its resistance to corrosion, and its ability to be successfully alloyed with various metals, hafnium was employed in several high temperature and aerospace applications. In addition, its large neutron absorption cross section makes it attractive for use in nuclear control rods, in particular, in nuclear submarine [1]. Hafnium has also found applications as filament material in electronic and electrical devices, as well as cutting tools, ceramics and fluoride glasses. However, its high melting temperature (2504 ± 20 K) and its reactivity with oxygen at very elevated temperature [1], make it problematic to measure the thermophysical properties of its superheated and undercooled phases using traditional methods. This motivated the use of containerless processing methods and non-contact diagnostic techniques. The electrostatic levitation furnace developed by the National Space Development Agency of Japan (NASDA) [2–8] circumvented the difficulties associated with high temperature processing and allowed an accurate and quick determination of the thermophysical properties of different metals [9–12]. High temperature processing was achieved in vacuum by using multiple laser heating beams, thus isolating the sample from contaminating walls as well as surrounding gases and providing sufficient stability for the thermophysical properties to be measured [7]. The facility also permitted deep undercooling of the levitated sample that was not heated by the electrostatic scheme because of containerless conditions and fast radiative cooling. Also, since the sample was free from any enclosure, it represented an easy target for various diagnostic detectors and probes.

An accurate knowledge of thermophysical properties and their temperature dependence is paramount for several basic studies on phase transformations, nucleation, atomic dynamics, surface physics, and related phenomena (Marangoni convection, etc.), as well as industrial processes, such as refining, bubble migration, forming, casting, and welding, to name but a few. These properties are also needed when designing new high performance alloys because the properties of an end member (e.g., binary, ternary systems, etc.) are required to estimate those of the final alloy. Moreover, the properties can sometimes be used to determine other thermophysical quantities. For example, enthalpy, entropy, and Gibbs free energy can be derived from the heat capacity.

Besides its use for thermophysical properties determination, this facility has a wide range of potential applications. For example, it can also be used to synthesize new materials, in particular, alloys with novel properties [13]. Although its best feature lies in its ability to handle corrosive liquids, it is also attractive for the study of solids that exhibit corrosive

activity at high temperature. A similar facility, currently under development by NASDA, will be dedicated to the analysis of the atomic structure of overheated and undercooled materials by neutron scattering experiments [14]. A pressurized version of the electrostatic levitation furnace, also under development, was recently successfully used to process ceramics and glass forming materials [15].

This paper successively describes the facility and the method of determining the thermophysical properties, and presents the experimental results. This work focuses on the properties of high temperature solid (β) and liquid hafnium, namely, the density, the thermal expansion coefficient, the constant pressure heat capacity, the hemispherical total emissivity, the surface tension and the viscosity. The value of the latent heat of fusion was also calculated.

2. EXPERIMENTAL SETUP AND PROCEDURES

2.1. Electrostatic Levitation Furnace

The measurements reported in this paper have been carried out using an electrostatic levitation furnace developed by NASDA [2–8]. The apparatus was based on a design by Rhim et al. [16] with modifications in the areas of sample levitation initiation, charging, handling, imaging, and heating configuration without which the described experiments would have been difficult to perform [6, 7]. Figure 1a illustrates schematically the electrostatic levitation furnace. The facility consisted of a stainless steel chamber which was evacuated to $\sim 10^{-5}$ Pa before the sample processing was initiated. The chamber housed the sample that was levitated between two parallel disk electrodes, typically 10 mm apart. These electrodes were used for vertical position sample control (z) (Fig. 1b). The positioning system relied on a set of orthogonally disposed He–Ne lasers and the associated position detectors. The sample position information was fed to a computer that inputs new values of z to a high voltage amplifier at a rate of 720 Hz so that a prefixed position could be maintained. In addition, four spherical electrodes distributed around the bottom electrode were used for horizontal control (x, y), also via a feedback loop. The lower electrode was also surrounded by four coils that generated a rotating magnetic field that was used for rotation control [17]. The top electrode was gimbaled by four micrometer screws, allowing accurate electrode balancing and separation. The bottom electrode had a central hole that permitted sample handling with the help of a molybdenum pedestal contained in a 10-sample capacity cartridge. To excite oscillations of the liquefied sample, an ac voltage was superimposed on the levitation voltage from the bottom electrode (Fig. 1a).

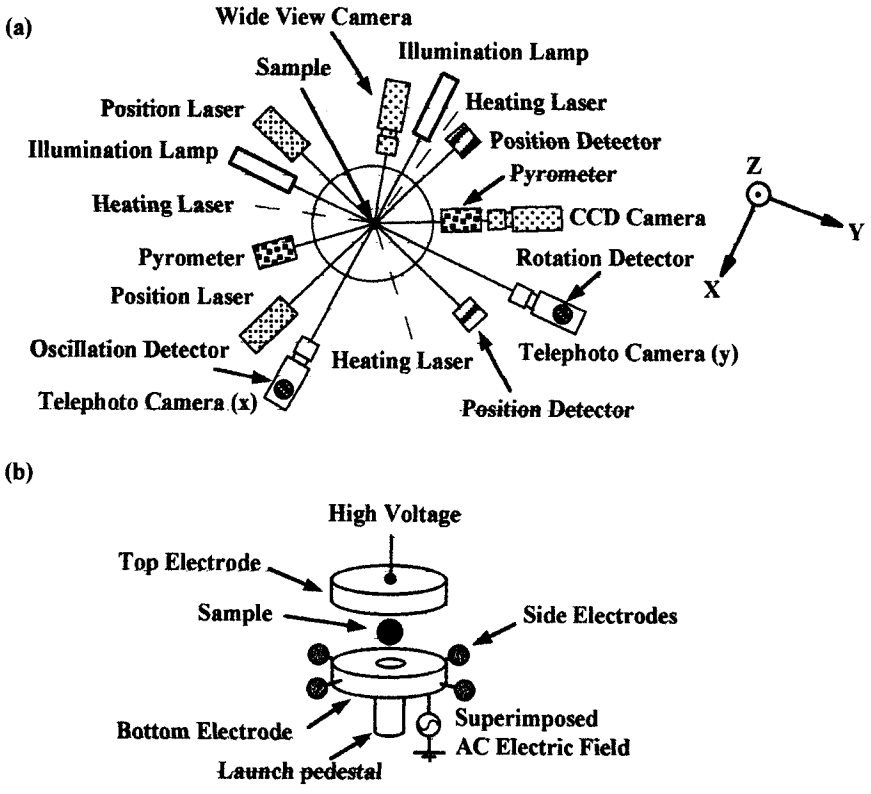

Fig. 1. Schematic view of NASDA'fs electrostatic levitation furnace (a) and electrode assembly (b).

For these experiments, specimens were prepared by arc melting 97 Wt. % purity hafnium wire (3% zirconium) (Nilaco Corporation, Tokyo, Japan) into spheroids with diameters of *ca.* 2 mm. Note that for simplicity, this material has been referred to as hafnium throughout the text.

Sample heating was performed using two 100 W CO_2 lasers (Synrad, Evolution 100) emitting at 10.6 μm. One beam was sent directly to the sample whereas the other beam was divided into two portions such that three focused beams, separated by 120 degrees, hit the specimen. Accurate computer control ensured that each beam delivered equal power to the sample. The heating configuration, together with controlled low frequency sample rotation (< 5 Hz), ensured good temperature homogeneity. Temperature data were obtained over a 1070 to 3800 K temperature interval using two automatic pyrometers (Chino Corp: Model IR-CS 2S CG,

operating at 0.90 μm and Model IR-AP, operating at 0.96 μm) with respective acquisition rates of 10 and 120 Hz.

The sample was observed by four charged-coupled-device (CCD) cameras. One camera offered a general view of both the electrode assembly and the sample. Another camera looked along the same path as a pyrometer to ensure constant alignment, to monitor the sample position in the horizontal plane, and to align the heating laser beams to minimize any detrimental photon pressure effects such as excessive rotation and oscillation on the levitated sample [18]. Control of rotation was of prime importance while measuring thermophysical properties such as density, surface tension, and viscosity since a sample deformed by rotation could lead to erroneous data [19]. Sample imaging for density determination was achieved by a high-resolution, black and white CCD video camera (Sony SSC-M370) equipped with a telephoto objective and a high-pass filter (450 nm), in conjunction with a high intensity ultraviolet background light. This gave a close look at the sample, allowing perimeter and surface features to be analyzed. The use of the ultraviolet lamp and the filter gave a background lighting efficiency that was practically independent of sample temperature (from an overheated liquid to a room temperature sample), yielding excellent imaging, thus allowing accurate determination of both density and the ratio of the constant pressure heat capacity and the hemispherical total emissivity [6]. A second high resolution CCD camera equipped with a telephoto objective in conjunction with a visible background light, located perpendicular to the other camera, was used to further help in aligning the laser beams and monitoring the sample position. In addition to the CCD cameras, each telephoto objective was equipped with a half-mirror, an interference filter (He–Ne emission line), and a detector. One of the detectors, coupled with a monochromator slit could determine the oscillating drop amplitude from the shadow of a He–Ne laser backlit sample and was dedicated to the measurement of the sample oscillation, from which the surface tension and viscosity could be determined [20]. The other sensor allowed the sample rotation rate to be measured by detecting the reflected He–Ne laser beam from its surface [17].

To initiate levitation, the sample, resting on the pedestal, was heated while monitoring its temperature with a pyrometer. The sample was heated with one beam while the two remaining beams converged at the location at which the sample was going to be positioned after the launch. Once the sample reached a temperature close to 1500 K, at which the thermionic emission was sufficient to charge the sample, the high voltage between the two electrodes was applied, and the feedback control software was activated. A few seconds later, the sample was launched into its normal

levitation position. The pre-heating laser beam was then redirected on the sample to ensure position stability and to increase the temperature. This procedure decreased dramatically the time required to bring a sample into a state at which its thermophysical properties can be measured, compared with other existing facilities [21].

2.2. Thermophysical Properties Determination

The vacuum version of NASDA's electrostatic levitation furnace was particularly attractive to measure the thermophysical properties (density, hemispherical total emissivity, surface tension, and viscosity) of high temperature hafnium. Since sample heating and levitation were independent, precise laser heating control allowed undercooled melts to be maintained for time scales much longer than those required for measurements. In addition, the spherical shape assumed by the levitated droplet (Fig. 2a) simplified the analysis.

Before the measurements were undertaken, a spheroid sample was first molten and re-solidified. This ensured that the pyrometer was correctly calibrated and aligned and that the sample, prepared by arc-melting, became truly spherical. In case the shape of a liquefied sample departed from that of a sphere during processing (due to excessive rotation), a counter torque was applied either with a magnetic field [17] or by appropriately steering the beams of the heating lasers [18] to restore the spherical shape. Hence, the measurements were taken only on spherical samples, whether they were in their solid or liquid phases.

The techniques used to determine the density and the quotient of constant pressure heat capacity over hemispherical total emissivity (C_p/ε_T) have been described in the literature and are summarized below [22, 23].

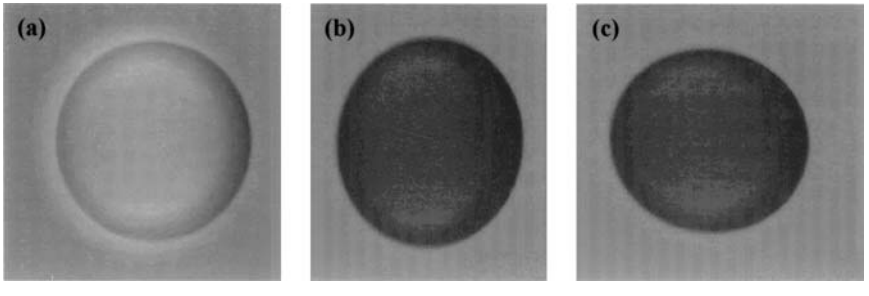

Fig. 2. Side view of a levitated and overheated hafnium-3 mass % zirconium sample without electrical excitation (2650 K) (a); side views of an undercooled sample (2330 K) undergoing electrical excitation (b, c).

Once the sample was molten (Fig. 2a), it took a spherical shape due to surface tension and the distribution of surface charge. Also, since the electrostatic scheme did not input any heat, a high temperature sample experienced pure radiative cooling when the heating laser beams were blocked and the resulting energy equation governing the cooling process reduced to

$$(mC_p/M)\, dT/dt = \varepsilon_T A\sigma(T^4 - T_{amb}^4) \tag{1}$$

where m is the sample mass, M is the molar mass, C_p is the constant pressure molar heat capacity, ε_T is the hemispherical total emissivity, A is the sample area, σ is the Stefan–Boltzmann constant, and T and T_{amb} are, respectively, the sample and ambient temperatures. The radiance temperature was measured by the pyrometers and was calibrated to true temperature using the known melting temperature of the sample ($T_m = 2504$ K). Calibration to true temperature was performed using custom-made Code Warrior™ software. A typical temperature profile for a cooling hafnium sample exhibiting a 285 K undercooling of the liquid phase, recalescence at the melting temperature (sudden temperature rise due to the release of the latent heat of fusion of an undercooled sample upon solidification), undercooling of the solid β-phase, and recalescence at the α-β allotropic phase transition temperature (2023 K), is shown in Fig. 3. After the sample started to cool, both the image and the cooling curve data could be used to measure simultaneously the density and the ratio of constant pressure heat capacity and hemispherical total emissivity. For density measurements, the recorded video images (Fig. 2a) were digitized and matched to the cooling curve. Then, NASDA-developed software extracted the area from each image. Since the sample was axi-symmetric and because its mass was known, the density could be found for each temperature. The ratio of constant pressure heat capacity and hemispherical total emissivity could be determined from Eq. (1) since all parameters were known, and since the area was found from the images and dT/dt from the cooling curve.

The surface tension and viscosity were measured by the oscillation drop technique, a method in which the frequency of the oscillation of levitated molten sample about its equilibrium shape was measured [24, 25]. This method was attractive as it allowed measurements in the metastable state of undercooled melts and on highly reactive materials. This technique was described elsewhere [20] and is explained below for completeness. To measure the surface tension using this method, a sample was first heated, became molten, and was brought to a selected temperature, while closely ensuring excellent position stability, no rotation conditions, and sample sphericity. Then, a $P_2\cos(\theta)$-mode drop oscillation was induced to the sample by superimposing a small sinusoidal electric field on

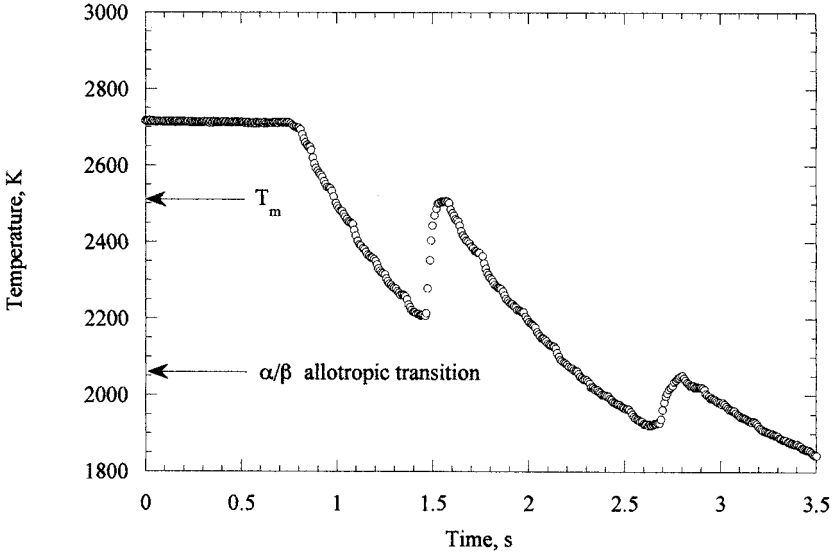

Fig. 3. Radiative cooling curve for hafnium-3 mass % zirconium showing undercooling and recalescences at the melting temperature and at the α-β allotropic phase transition temperature.

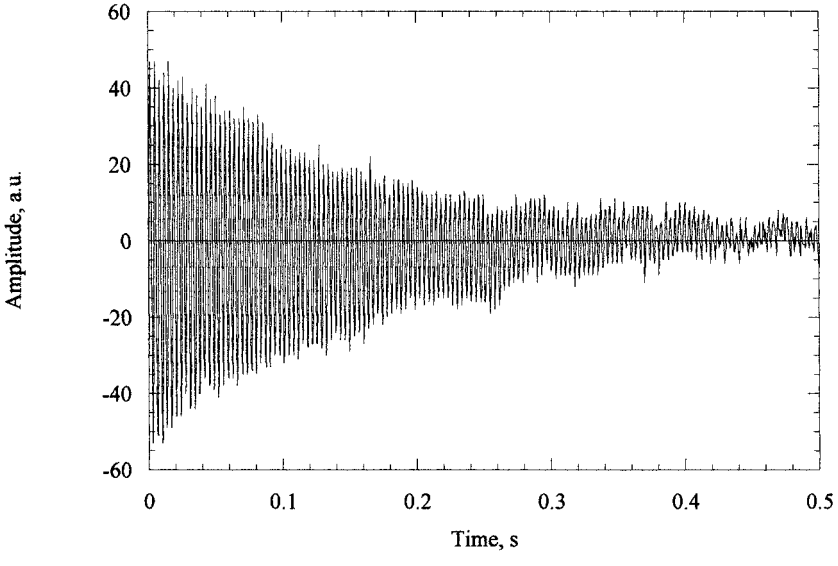

Fig. 4. Typical signal of the decay of the oscillation following electrical excitation.

the levitation field. Figures 2b and c show side views of a supercooled levitated molten hafnium sample subject to such an electrical excitation. The transient signal which followed the termination of the excitation field was detected and analyzed using NASDA-developed LabVIEW™ software. A typical signal of the decay of the oscillation is shown in Fig. 4. This was done numerous times at a given temperature and repeated for several temperatures. Using the characteristic oscillation frequency ω_c of this signal after correcting for nonuniform surface charge distribution [26], the surface tension σ can be found from the following equation [20],

$$\omega_c^2 = (8\sigma/r_o^3\rho)[1-(Q^2/64\pi^2 r_o^3 \sigma e_o)][1-F(\sigma, q, e)] \tag{2}$$

where

$$F(\sigma, q, e) = [243.31\sigma^2 - 63.14q^2\sigma + 1.54q^4]\, e^2 / [176\sigma^3 - 120q^2\sigma^2 + 27sq^4 - 2q^6], \tag{3}$$

r_o is the radius of the sample when it assumes a spherical shape, ρ is the liquid density, Q is the drop charge, ε_o is the permittivity of vacuum, and q and e are defined by

$$q^2 = Q^2/(16\pi^2 r_o^3 e_o) \tag{4}$$

and

$$e^2 = E^2 r_o \varepsilon_o \tag{5}$$

respectively, with E being the applied electric field. Similarly, using the decay time τ given by the same signal, the viscosity η was found by

$$\eta = \rho r_o^2/(5\tau). \tag{6}$$

From Eqs. (2) and (6), it can be seen that both the surface tension and the viscosity depend on the sample radius and density. For density, we simply substituted our previously determined data in these equations. Although the vapor pressure of hafnium was rather low, it was decided to monitor the radius variation in time by imaging to insure that the measured properties were not distorted by sample evaporation, instead of relying purely on measurements of the mass of the sample before and after the experiment, as done elsewhere [20]. Hence, a real-time value of the radius was used. A forthcoming paper will explain this procedure in detail, showing in particular how it can be applied to measure the vapor pressure of high temperature liquid materials [8].

3. EXPERIMENTAL RESULTS

3.1. Density

The results for the density measurements of hafnium, shown in Fig. 5, exhibit a discontinuity at the melting temperature, characteristic of a first-order transition. For the liquid phase, the measurements were taken over the 2220 to 2875 K temperature range and covered the undercooled region by nearly 300 K. The density, as for that of other pure metals, exhibited a linear behavior as a function of temperature and can be fitted by the following equation:

$$\rho_L(T) = 1.20 \times 10^4 - 0.44(T - T_m)\ (\mathrm{kg \cdot m^{-3}}) \qquad (2220 \text{ to } 2875 \text{ K}) \quad (7)$$

where T_m is the melting temperature (2504 K). In this experiment, the uncertainty of the measurements was estimated to be less than 2 per cent from the resolution of the video grabbing capabilities (640×480 pixels) and from the uncertainty in mass measurement (± 0.0001 g). To our knowledge, these measurements were the first to be reported that included such a large temperature span into the undercooled region. The values that appeared in the literature are summarized in Table I for comparison. Our value is in

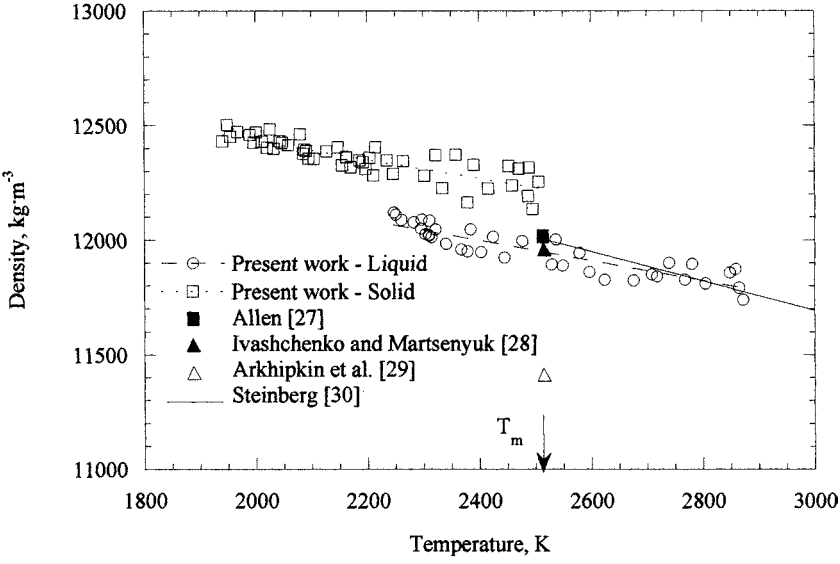

Fig. 5. Density of hafnium-3 mass % zirconium versus temperature.

Table I. Literature Values of the Density of Hafnium-3 mass % Zirconium ("s" denotes data for the solid β-phase)

Density @T_m (10^3 kg·m^{-3})	Temperature Coeff. (K^{-1})	Temperature (K)	Reference	Technique
12.0	−0.44	2220–2875	Present work	levitation
12.2^s	−0.41	1950–2500	Present work	levitation
12.0	—	2504	Allen [27]	calculated
11.97	—	2504	Ivashchenko et al. [28]	drop weight
11.4	—	2504	Arkhipkin et al. [29]	drop weight
12.0	−0.63	2504	Steinberg [30]	calculated

perfect agreement with that calculated by Allen [27] from room-temperature specific volumes increased for cubical thermal expansion to the melting point and an estimated amount for fusion. It agrees, within experimental errors, with that measured by Ivashchenko et al. [28] and is 5.5% higher than that obtained by Arkhipkin et al. [29], both using the drop weight technique in vacuum. Our temperature coefficient was nearly 30% lower than that calculated by Steinberg [30].

The volume variation $V_L(T)$ of the molten state, normalized with the volume at the melting temperature V_m, was derived from Eq. (7), and could be expressed by

$$V_L(T)/V_m = 1 + 3.7 \times 10^{-5}(T - T_m) \qquad (2220 \text{ to } 2875 \text{ K}) \qquad (8)$$

where 3.7×10^{-5} represents the volume expansion coefficient $\alpha_L(T)$.

The small discrepancy observed between our result and that of Arkhipkin et al. [29] could be attributed to the difference in processing techniques and the extent to which evaporation losses have been considered. We used a containerless approach in high vacuum, isolating our samples from container walls and gases, whereas the other investigator used a method for which possible chemical reactions between the highly reactive molten hafnium and residual gases could have altered the final density values.

Figure 5 also illustrates the density measurements for the solid β-phase over the 1950 to 2500 K temperature range. It covers the undercooled β-phase by nearly 65 K. Again, a linear behavior was observed and the data can be fitted by the following relation:

$$\rho_S(T) = 1.22 \times 10^4 - 0.41(T - T_m) \text{ (kg·m}^{-3}) \qquad (1950 \text{ to } 2500 \text{ K}) \qquad (9)$$

where T_m is the melting temperature. We believe that these were the first data to be reported for the density of high temperature and undercooled solid β-hafnium.

From Eq. (9), the volume variation $V_S(T)$ of the solid β-phase, normalized with respect to the volume at the melting temperature V_m, can be derived and expressed as

$$V_S(T)/V_m = 1 + 3.4 \times 10^{-5}(T - T_m) \qquad (1950 \text{ to } 2500 \text{ K}) \qquad (10)$$

where 3.4×10^{-5} is the volume expansion coefficient $\alpha_S(T)$.

3.2. Constant-Pressure Heat Capacity

The ratio between the constant-pressure heat capacity and the hemispherical total emissivity as a function of the temperature is shown in Fig. 6 for both solid and liquid hafnium. For the liquid state, $C_{PL}(T)/\varepsilon_{TL}(T)$ is nearly constant with temperature and can be linearly fitted as

$$C_{PL}(T)/\varepsilon_{TL}(T) = 133.09 + 3.15 \times 10^{-3}(T - T_m)\ (\text{J} \cdot \text{mol}^{-1} \cdot \text{K}^{-1})$$
$$(2250 \text{ to } 2650 \text{ K}). \qquad (11)$$

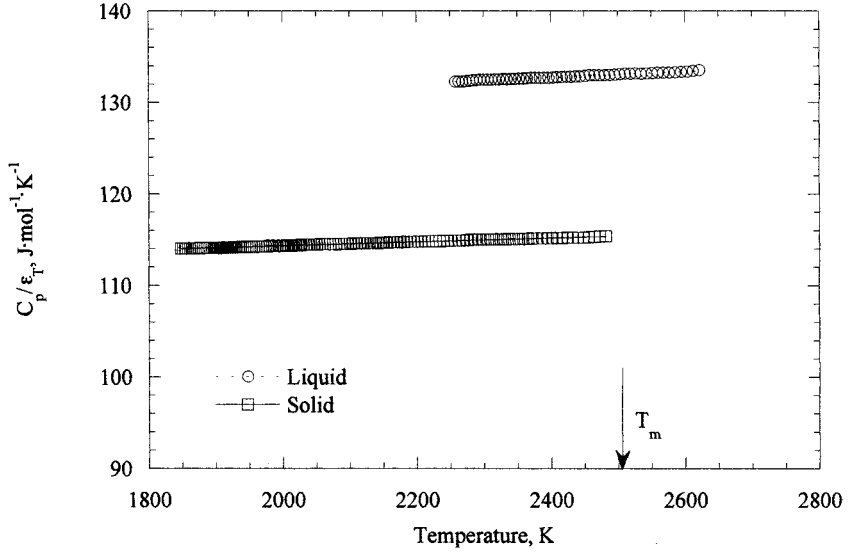

Fig. 6. Ratio between the constant-pressure heat capacity and the hemispherical total emissivity of hafnium-3 mass % zirconium versus temperature.

When the value of C_{PL} given by Hultgren et al. [31] at the melting temperature was used ($33.47\,J\cdot mol^{-1}\cdot K^{-1}$), ε_{TL} could be determined from Eq. (11) and was equal to 0.25. Although changes in peak emission wavelength with temperature might affect the value of total emissivity as a function of temperature, the lack of data for the overheated and undercooled states of hafnium prompted us to assume that $\varepsilon_{TL}(T)$ remained constant at a value of 0.25 over the whole temperature range. The temperature dependence of $C_{PL}(T)$ could then be determined from Eq. (11) by simply multiplying it by $\varepsilon_{TL}(T) = 0.25$. The heat capacity so obtained (Fig. 7) can be expressed by the following equation:

$$C_{PL}(T) = 33.47 + 7.92\times 10^{-4}(T - T_m)\ (J\cdot mol^{-1}\cdot K^{-1}) \qquad (2250 \text{ to } 2650\ K). \tag{12}$$

Figure 7 also shows the ratio between constant-pressure heat capacity and the hemispherical total emissivity as a function of the temperature for solid (β) hafnium. As for the liquid state, the trend was nearly constant with temperature and can be fitted as

$$C_{PS}(T)/\varepsilon_{TS}(T) = 115.43 + 2.17\times 10^{-3}(T - T_m)\ (J\cdot mol^{-1}\cdot K^{-1}) \qquad (1850 \text{ to } 2500\ K). \tag{13}$$

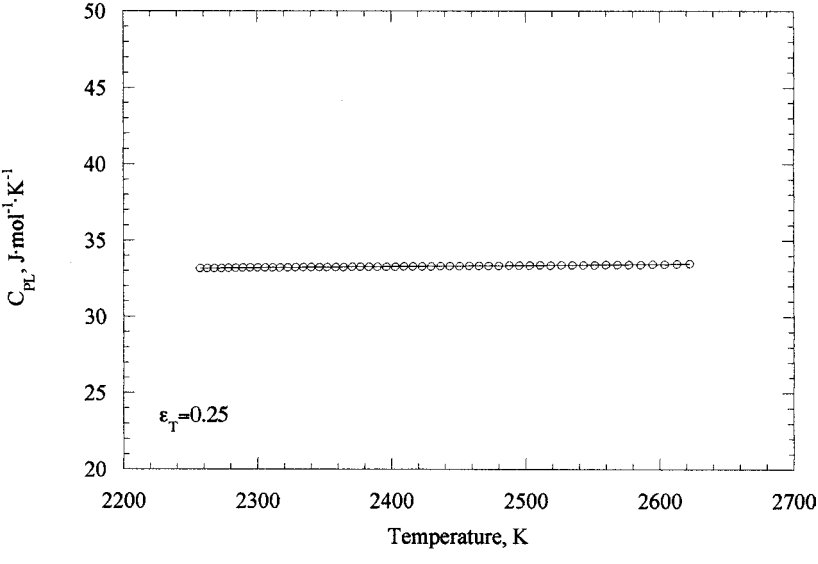

Fig. 7. Heat capacity of liquid hafnium-3 mass % zirconium versus temperature, calculated using the data from Fig. 6 and $\varepsilon_{TL}(T) = 0.25$.

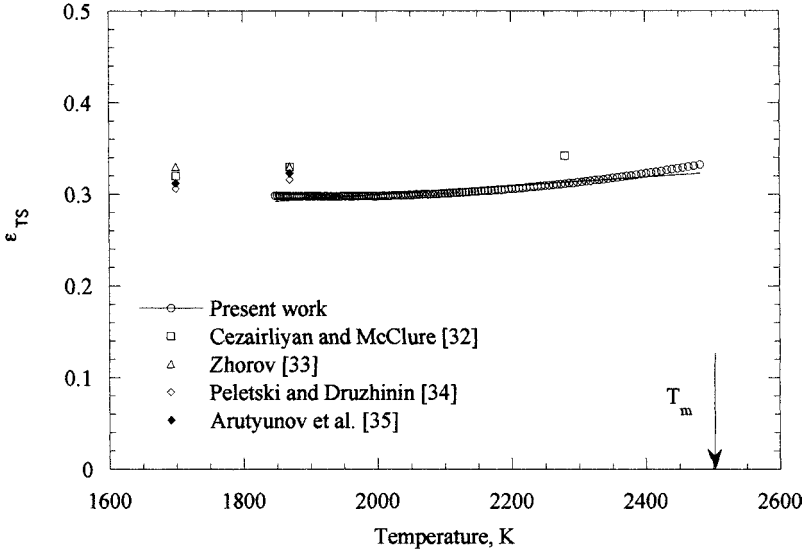

Fig. 8. Hemispherical total emissivity of solid hafnium-3 mass % zirconium versus temperature, calculated using the data from Fig. 6 and $C_{PL}(T)$ from Ref. 32.

Similarly, using the values of $C_{PS}(T)$ given by Cezairliyan et al. [32] for the β-phase, it was possible to obtain $\varepsilon_{TS}(T)$, which can be expressed as (Fig. 8)

$$\varepsilon_{TS}(T) = 0.32 + 4.79 \times 10^{-5}(T - T_m) \qquad (1850 \text{ to } 2500 \text{ K}). \qquad (14)$$

Our values of ε_{TS} over temperature are consistently lower than those reported by earlier investigators. For example, at $T = 1870\ K$, our value is 12% lower compared with that obtained by Cezairliyan et al. [32] with the pulse heating technique and by Zhorov [33] with an electrical resistivity scheme. Our value is also 8.2% lower than that of Peletskii et al. [34], and 10% lower than that obtained by the tube method by Arutyunov et al. [35]. Although the other investigators obtained only a few data points, the trend of their temperature coefficient with ours is similar. Besides the difference in composition [33–35], we believe that a few other reasons could explain such discrepancies. Because our sample was solidified from a deeply undercooled state, it is possible that its surface structure might be finer than that of other authors, which could have led to a different emissivity value. In addition, the slow reading capability of our pyrometer might have induced a shift in the temperature dependence of the emissivity.

The latent heat of fusion has also been determined by adding the enthalpy contributions of the undercooled liquid and that of the isothermal

Table II. Literature Values of the Latent Heat of Fusion of Hafnium-3 mass % Zirconium

Enthalpy of fusion ($kJ \cdot mol^{-1}$)	Reference	Technique
15.1	Present work	levitation
24.06	Kubaschewski et al. [36]	calculated

region following the recalescence (see Fig. 3). The contribution of the undercooled portion was found by integrating $C_{PL}(T)$ over temperature from T_m to the lowest temperature of undercooling, whereas that of the isothermal solid was obtained by integrating $\varepsilon_{TS} A\sigma(T^4 - T^4_{amb})$ over the time at which the solid stays at T_m. The latent heat of fusion was found to be equal to 15.1 $kJ \cdot mol^{-1}$ which is considerably lower than the theoretical value reported by Kubaschewski et al. [36] (Table II). The difference could, in part, be attributed to the slow response of our pyrometer, which lags the recalescence phenomenon, thus inducing errors in time and in uncertainties in $C_{PL}(T)$ or ε_{TS}.

3.3. Surface Tension

Previous experiments with tin samples showed that patches of oxides floating on a liquid sample could be easily detected either visually with telephoto cameras or with our He–Ne laser based sample rotation detection system. No such oxide or nitride patches were either tracked by the rotation detection or by visual observation when the hafnium sample was liquified.

Our results for the surface tension have been plotted in Fig. 9. The surface tension of hafnium, as that of other pure metals, exhibited a linear nature as a function of temperature. In this experiment, the uncertainty of the measurements was estimated to be better than 5 percent from the response of the oscillation detector and from the density measurements. The data available from the literature are also superimposed on the same figure for comparison. In addition, Table III summarizes the existing surface tension data with a corresponding temperature range of applicability and measurement technique. The surface tension (Fig. 9), measured over the 2220 to 2675 K temperature range and covering the undercooled region by 285 K, can be expressed by

$$\sigma(T) = 1.614 \times 10^3 - 0.100(T - T_m)\ (mN \cdot m^{-1}) \qquad (2220 \text{ to } 2675\ K) \qquad (15)$$

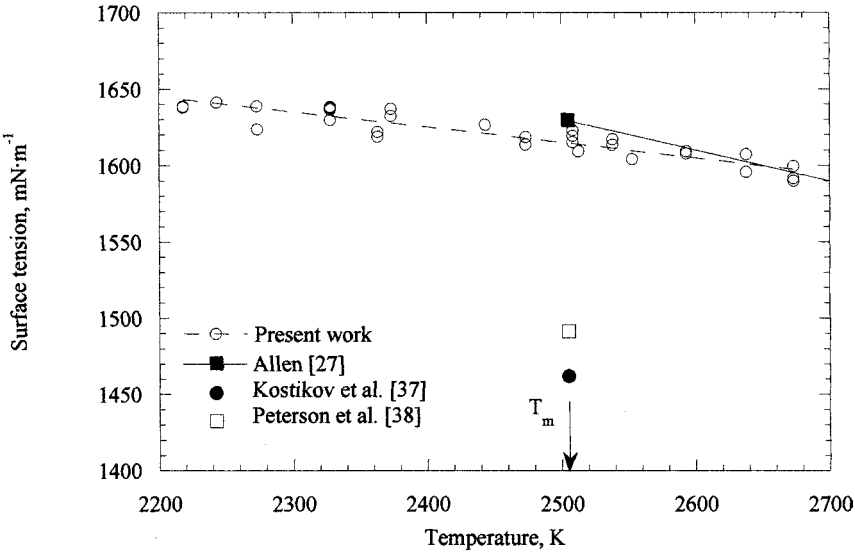

Fig. 9. Surface tension of hafnium-3 mass % zirconium versus temperature.

where T_m is the melting temperature. These measurements were the first to cover a large temperature interval. At the melting temperature, our result is, within experimental errors, identical with that obtained by Allen [27] with the pendant drop technique. It is over 8 percent higher compared with that reported by Kostikov et al. [37] using the pendant drop method, and over 10 percent higher than that measured by Peterson et al. [38] using the drop weight method. Our temperature coefficient is however nearly half of that calculated by Allen [27].

The discrepancies between our results and those reported by other investigators [27, 37, 38] could stem from the difference in processing techniques. In this work, containerless levitation in high vacuum and radiative heating isolated the samples from container walls and gases, whereas the above authors employed the pendant drop or drop weight

Table III. Literature Values of the Surface Tension of Hafnium-3 mass % Zirconium

Surface Tension @T_m ($mN \cdot m^{-1}$)	T. Coeff. (K^{-1})	Temperature (K)	Reference	Technique
1614	−0.100	2220–2675	Present work	levitation
1630	−0.21	2504	Allen [27]	pendant drop
1490	—	2504	Kostikov et al. [37]	pendant drop
1460	—	2504	Peterson et al. [38]	drop weight

methods for which possible chemical reactions between the highly reactive molten metal and a support could have occurred. In addition, electron bombardment and induction heating, used by the above authors, might have been accompanied with some evaporation from the electrodes or from the heating elements, thus further contaminating the specimen under study. This could have affected the surface tension, highly dependent upon contamination and might explain why the results of Refs. 37 and 38, obtained with non-containerless techniques, are lower than our. Purity of the samples and the level of vacuum could also explain the discrepancies between our data and those obtained by other investigators.

3.4. Viscosity

By extracting the decay time component from the decay of the oscillation of a sample, used to measure the surface tension (Fig. 4), it was possible to determine the viscosity of hafnium over the same temperature range. Figure 10 shows that the viscosity of hafnium, as other thermophysical properties reported, exhibits a linear trend as a function of temperature. Superimposed on the graphs is the datum obtained by Agaev et al. [39], the only other value found in the literature. The temperature dependence of the viscosity of overheated and undercooled hafnium is illustrated

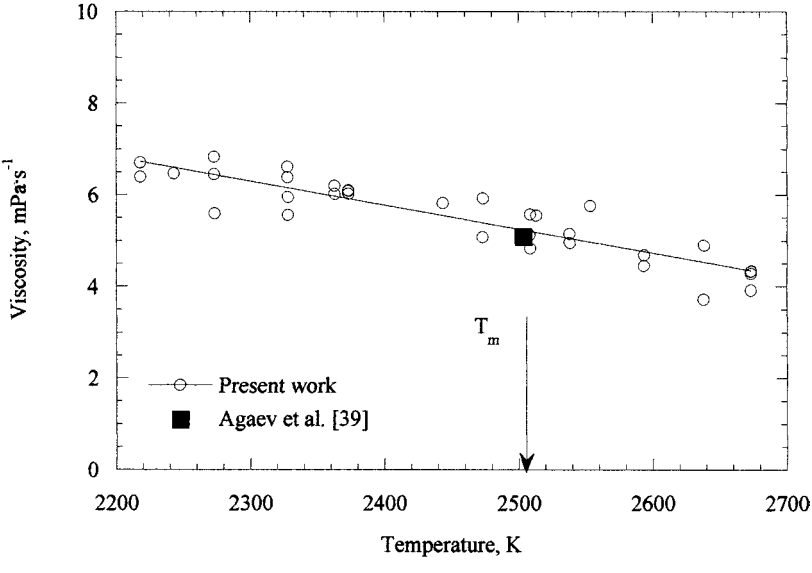

Fig. 10. Viscosity of hafnium-3 mass % zirconium versus temperature.

Table IV. Literature Values of the Viscosity of Hafnium-3 mass % Zirconium

Viscosity @T_m (mPa s)	T. Coeff. (K^{-1})	Temperature (K)	Reference	Technique
5.23	−0.00524	2220–2675	Present work	levitation
5.0	—	2504	Agaev et al. [39]	capillary

in Fig. 10 over the 2220 to 2675 K range. The data can be fitted by the following Arrhenius function:

$$\eta(T) = 0.495 \exp[48.65 \times 10^3/(RT)] \text{ (mPa} \cdot \text{s)} \qquad \text{(2220 to 2675 K)} \qquad (16)$$

where R, the gas constant, is equal to 8.31 $\text{J} \cdot \text{mol}^{-1} \cdot \text{K}^{-1}$. At the melting temperature, it compares within 5 percent with that published by Agaev et al. using the capillary technique [39] (Table IV). The discrepancy might be explained by the contamination generated by the capillary and also by the difference in specimen purities.

5. CONCLUSIONS

We have presented numerous thermophysical properties of solid and liquid hafnium measured using the electrostatic levitation furnace developed by NASDA. For the first time, we report the density of liquid hafnium over a wide temperature range that includes the undercooled state. Also given are the thermal expansion coefficient of both solid and liquid hafnium and the density of its solid phase over a large temperature span. In addition to the latent heat of fusion, the results of the ratio of constant-pressure heat capacity to the hemispherical total emissivity of the liquid and solid phases are presented in this paper. The surface tension and viscosity of hafnium are also reported for the first time over large temperature intervals that include the supercooled phase.

Several thermophysical data presented in this work were obtained either from radiative cooling curves or image acquisition. Therefore, to improve our data, efforts are being focused towards ways to increase image sharpness, resolution, and contrast. Emphasis should also be directed to devise better numerical techniques to get dT/dt from the cooling curves to minimize numerically induced errors, when obtaining C_P/ε_T. Current efforts are also devoted to designing a custom-made, fast-response pyrometer to capture more precisely the recalescence phenomenon. In addition to the imaging technique used to monitor the sample radius variation during processing, the surface tension and the viscosity measurements relied on the

analysis of the induced sample oscillations. Hence, ways to improve signal acquisition and amplification are also sought.

Present activities target on the measurements of similar properties of other refractory metals such as tantalum, rhenium, and tungsten in their overheated and undercooled states. There are also hopes that modification of the measurement techniques could be applied to low viscosity dielectric oxide ceramic and glass forming materials in conjunction with the novel hybrid electrostatic-aerodynamic levitation furnace recently developed by NASDA [14].

ACKNOWLEDGMENTS

The authors would like to thank Dr. T. Matsumoto (National Research Laboratory of Metrology, Japan) for bringing to our attention the paper by Cezairliyan. We would also wish to acknowledge Dr. J. Yu for his careful reading of the manuscript and Mrs. Ebihara for her thorough literature search. Sincere thanks are also directed to Dr. Aoyama for his help in the data-taking process and to Dr. Y. Arai, and Dr. N. Koshikawa for discussions.

REFERENCES

1. D. R. Lide and H. P. R. Frederikse, eds., *CRC Handbook of Chemistry and Physics*, 78th ed. (CRC Press, Boca Raton, Florida, 1997).
2. P.-F. Paradis, T. Ishikawa, and S. Yoda, in *Proc. Spacebound 2000*, Vancouver, British Columbia, Canada (2001).
3. T. Ishikawa, P.-F. Paradis, and S. Yoda, *J. Jpn. Soc. Microg. Appl.* **17**:98 (2000).
4. P.-F. Paradis, T. Ishikawa, and S. Yoda, in *Proc. First Int. Symp. Microgravity Res. Applications in Phys. Sci. and Biotech.*, Sorrento, Italy, September 2000 (ESA SP-454) (2001), p. 993.
5. T. Ishikawa, P.-F. Paradis, and S. Yoda, *J. Jpn. Soc. Microg. Appl.* **18**:106 (2001).
6. T. Ishikawa, P.-F. Paradis, and S. Yoda, *Rev. Sci. Instrum.* **72**:2490 (2001).
7. P.-F. Paradis, T. Ishikawa, and S. Yoda, *Space Technol.* (in press).
8. P.-F. Paradis, T. Ishikawa, and S. Yoda, submitted to *Euro. Phys. J. Appl. Phys.*
9. P.-F. Paradis, T. Ishikawa, and S. Yoda, *J. Mater. Sci.* **36**:5125 (2001).
10. T. Ishikawa, P.-F. Paradis, and S. Yoda, *Proc. 2nd Pan-Pacific Basin Workshop on Microgravity Sciences*, TP-1019, Pasadena, California, 2001 (in press).
11. P.-F. Paradis, T. Ishikawa, and S. Yoda, *Int. J. Thermophys.* **23**:555 (2002).
12. P.-F. Paradis, T. Ishikawa, and S. Yoda, *Int. J. Thermophys.* **23**:825 (2002).
13. J. Yu, P.-F. Paradis, T. Ishikawa, S. Ozawa, T. Saito, T. Motegi, and S. Yoda, *Japan. J. Appl. Phys.* **41**:2908 (2002).
14. P.-F. Paradis, T. Ishikawa, and S. Yoda, *Proc. of the LAM 11 Conf. Yokohama, Japan, Sept. 2001, J. Non-Cryst. Solids* **309**:312–314 (2002).
15. P.-F. Paradis, T. Ishikawa, J. Yu, and S. Yoda, *Rev. Sci. Instrum.* **72**:2811 (2001).
16. W.-K. Rhim, S.-K. Chung, D. Barber, K.-F. Man, G. Gutt, A. A. Rulison, and R. E. Spjut, *Rev. Sci. Instrum.* **64**:2961 (1993).

17. W.-K. Rhim and T. Ishikawa, *Rev. Sci. Instrum.* **69**:3628 (1998).
18. W.-K. Rhim and P.-F. Paradis, *Rev. Sci. Instrum.* **70**:4652 (1999).
19. W.-K. Rhim and T. Ishikawa, *Rev. Sci. Instrum.* **72**:3572 (2001).
20. W.-K. Rhim, K. Ohsaka, P.-F. Paradis, and R. E. Spjut, *Rev. Sci. Instrum.* **70**:2796 (1999).
21. W.-K. Rhim, California Institute of Technology, private communication.
22. S.-K. Chung, D. B. Thiessen, and W.-K. Rhim, *Rev. Sci. Instrum.* **67**:3175 (1996).
23. A. A. Rulison and W.-K. Rhim, *Rev. Sci. Instrum.* **65**:695 (1994).
24. S. Sauerland, G. Lohofer, and I. Egry, *J. Non Cryst. Solids* **156–158**:833 (1993).
25. Lord Rayleigh, *Proc. R. Soc. London.* **14**:184 (1882).
26. J. Q. Feng and K. V. Beard, *Proc. R. Soc. London. A* **430**:133 (1990).
27. B. C. Allen, *Trans. AIME* **227**:1175 (1963).
28. Yu. Ivashchenko and P. S. Martsenyuk, Zavod. Lab. (USSR) 39, 1, 42 (1973).
29. V. I. Arkhipkin, V. I. Kostikov, G. A. Grigorjev, and A. D. Agaev, in *Fiz. Khim. Granits Razdela Kontaktiryuschikh Faz.*, V. N. Eremenko, ed. (Naukova Dumka-Kiev, USSR, 1976), pp. 74–77.
30. D. J. Steinberg, *Metall. Trans.* **5**:1341 (1974).
31. R. Hultgren, R. L. Orr, R. L. Anderson, and K. K. Kelley, *Selected Values of Thermodynamic Properties of Metals and Metals* (Wiley, New-York, 1974).
32. A. Cezairliyan and J. L. McClure, *J. Res. Nat. Bur. Stand. (U.S.) Phys. and Chem.* **79A**:431 (1975).
33. G. A. Zhorov, *High Temp. (USSR)* **8**:501 (1970).
34. V. E. Peletskii and V. P. Druzhinin, *High Temp. (USSR)* **9**:490 (1971).
35. A. V. Arutyunov, S. N. Banchila, and L. P. Filippov, *High Temp. (USSR)* **10**:375 (1972).
36. O. Kubaschewski, and C. B. Alcock, *Metallurgical Thermochemistry*, 5th ed. (Pergamon Press, Oxford, 1979).
37. V. I. Kostikov, G. A. Grigorjev, V. I. Arkhipkin, and A. D. Agaev, *Izv. Vyss. Uch. Sav. Chern. Met. (USSR)* **3**:25 (1972).
38. A. W. Peterson, H. Kedesdy, P. H. Keck, and E. Scharz, *J. Appl. Phys.* **28**:213 (1958).
39. A. D. Agaev, V. I. Kostikov, and V. N. Bobkovskii, *Izv. Akad. Nauk. SSSR Met.* **3**:43 (1980).